Journal of Geophysical Research: Atmospheres

RESEARCH ARTICLE
10.1029/2018JD029326

Evaluating Soil Moisture Feedback on Convective Triggering: Roles of Convective and Land-Model Parameterizations

Ian N. Williams[1]

[1]Climate and Ecosystem Sciences Division, Lawrence Berkeley National Laboratory, Berkeley, CA, USA

Key Points:
- Surface and atmospheric controls on convective triggering can be identified using experiments with a single-column climate model
- Modeled responses of convective triggering to soil moisture are strongly influenced by convective cloud and land-surface parameterizations
- Parameterizations that permit soil moisture-triggering feedback mechanisms better predict statistics of daytime shallow and deep cumulus

Correspondence to:
I. N. Williams,
inwilliams@lbl.gov

Citation:
Williams, I. N. (2019). Evaluating soil moisture feedback on convective triggering: Roles of convective and land-model parameterizations. *Journal of Geophysical Research: Atmospheres*, *124*, 317–332. https://doi.org/10.1029/2018JD029326

Received 13 JUL 2018
Accepted 27 NOV 2018
Accepted article online 7 DEC 2018
Published online 15 JAN 2019

©2018. American Geophysical Union. All Rights Reserved.

Abstract Feedbacks between soil moisture and convective precipitation are not well represented in current Earth system models, and can affect projections of drought and heavy-precipitation extremes. To explore the atmospheric and land-surface influences on the initiation (triggering) of daytime deep convection, single-column model experiments were performed using the NCAR Community Earth System Model (CESM1.2), over the U.S. Southern Great Plains. The results indicate that the positive and negative feedback mechanisms found in earlier studies (using simplified boundary-layer models) are robust to large-scale forcing and interactions between boundary-layer turbulence, cloud dynamics, and radiation. However, systematic responses of convective triggering to soil moisture emerged only after switching from a convective available potential energy-based to a convective inhibition energy-based convective parameterization. This suggests that the choice of convective mass-flux closure largely determines the sensitivity of parameterized convective clouds to land-surface state. Errors in land-model parameterizations of evapotranspiration also affect the probability of deep convection, with vegetation (transpiration) playing an important role in linking soil moisture to surface energy partitioning and clouds. Parameterizations that permit the triggering feedback mechanism better predict the statistics of daytime shallow and deep convection, with respect to observations from the Atmospheric Radiation Measurement site in the Southern Great Plains. The results illustrate how errors in the representation of evapotranspiration in land-surface models can propagate through the chain of coupled land-atmosphere processes to affect convective clouds.

1. Introduction

The parameterization of deep convection is a major source of uncertainty in climate model projections of future changes in the water cycle over land (Klein et al., 2006; Qian et al., 2015; Qiao & Liang, 2017; Van Weverberg et al., 2015; Wilcox & Donner, 2007; Yang et al., 2013). A related source of uncertainty is the parameterization of evapotranspiration (ET) and its relationship to soil moisture and vegetation state (Cheruy et al., 2014; Y. Lin et al., 2017; I. N. Williams et al., 2016). In particular, poor representation of the feedback between soil moisture and precipitation can contribute to the persistence and amplification of climate prediction biases (Bonan & Levis, 2006; Boussetta et al., 2015). Existing models may fail to correctly predict the sign of the soil moisture-precipitation feedback (Hohenegger et al., 2009). An important component of this feedback is the response of convective triggering (the initiation of deep convection via production of buoyant cloudy air) to temporal variations in soil moisture, mediated by the coupling between soil moisture, surface energy fluxes, boundary-layer state, and clouds (Dirmeyer, 2011; Dirmeyer et al., 2014; Santanello et al., 2017). We refer to this chain of processes as the triggering feedback, in contrast to the feedback involving changes in precipitation amount (Findell et al., 2011; Schär et al., 1999).

A primary challenge in evaluating the triggering feedback (in models or observations) is that the sign of the feedback varies with atmospheric state. One-dimensional (1-D) boundary-layer models (Ek & Holtslag, 2004; Findell & Eltahir, 2003; Gentine et al., 2013) show that triggering is more likely over wet soil in tropospheric states known as wet soil-moisture advantage regimes, consistent with a positive feedback; while triggering is more likely over dry soil in dry-advantage regimes, consistent with a negative feedback. Thus, simple averaging of triggering events over days with wetter versus drier soil could conceal the responses of convective triggering to soil moisture by averaging them out across different regimes. An important question is how to extend the boundary-layer model results of Findell and Eltahir (2003; hereafter FE03) to infer wet- and dry-soil moisture advantage regimes from observations (Ferguson & Wood, 2011; Roundy et al., 2012; H. -J. Song et al., 2016). Conditional averaging of such regimes could then be used to reveal the responses of convective triggering to soil moisture variations.

Another challenge is to isolate the effects of soil moisture from those of large-scale weather systems. A well-known approach is to perform soil moisture perturbation experiments in climate models (Koster et al., 2003, 2006) or simplified boundary-layer models (Ek & Holtslag, 2004; Findell & Eltahir, 2003; Gentine et al., 2013). Such controlled experiments are effective in identifying causal relationships, but are subject to errors in model representation of convective clouds (Chen et al., 2017; Sun & Pritchard, 2016), boundary-layer turbulence (Santanello et al., 2011), and ET (I. N. Williams et al., 2016).

On the other hand, empirical approaches have shown evidence for positive (Findell et al., 2011; Roundy et al., 2012) or negative triggering feedbacks (Taylor et al., 2012) or both (Ferguson & Wood, 2011), depending in part on the temporal and spatial scales represented by the analyses (Guillod et al., 2015). However, such approaches can be confounded by covarying factors such as low-level jets and related large-scale meteorological forcing (Wang et al., 2015), and vegetation processes. For example, correlations based only on soil moisture can underestimate the role of the land-surface in cloud and precipitation processes, since vegetation state (e.g., leaf area index, LAI) can also influence surface heat fluxes (Guillod et al., 2014; I. N. Williams et al., 2016; I. N. Williams & Torn, 2015). New approaches that integrate observations and complex models are ultimately needed to address causality, and to inform development of model parameterizations.

The transition from shallow to deep cumulus convection depends in part on surface energy partitioning (Couvreux et al., 2012; Gentine et al., 2013; Y. Zhang & Klein, 2010, 2012). The surface evaporative fraction (EF) is a measure of this partitioning, defined as the ratio of latent heat flux to the sum of sensible and latent heat flux. Higher sensible heating (lower EF) promotes greater boundary layer (PBL) growth and entrainment (Santanello et al., 2017). Based on the boundary-layer model results of FE03, we expect dry-advantage regimes to be characterized by drier environments for which surface evaporation alone would be insufficient for air parcels to reach saturation and buoyancy. In such environments, saturation is favored by deeper PBLs and thus greater adiabatic cooling of air parcels. In contrast, we expect wet-advantage regimes to be characterized by more humid but stratified environments, in which the ability of parcels to achieve saturation and buoyancy is limited in deeper PBLs due to entrainment of warmer air, which reduces the relative humidity at the PBL top (Berg et al., 2013; Betts, 2007; Ek & Holtslag, 2004; Eltahir, 1998; Findell & Eltahir, 2003; Gentine et al., 2013).

This study revisits the experimental approach of FE03, using a single-column climate model (SCM). As described in detail in section 2, our SCM configuration represents several processes not included in the boundary-layer model used in FE03; such as the effects of large-scale forcing, in terms of prescribed advective tendencies and vertical velocities; parameterized cloud dynamics based on entraining plume models; realistic radiative transfer including interactions with surface fluxes; and biogeophysical controls on ET via coupling of transpiration to stomatal conductance and photosynthesis. The present work does not attempt to validate a modeling framework as a surrogate for observations, but rather to explore combinations of model parameterizations that differ in their representation of soil moisture impacts on triggering.

This study is motivated by the perspective that different land-model and convective cloud parameterizations can represent different hypotheses for soil moisture-precipitation feedbacks, which can be tested against observations. The objectives are to identify observable signatures of triggering feedbacks in models and to test the underlying hypotheses by comparing those signatures to observations.

2. Approach

The NCAR Community Earth System Model (CESM1.2.2; Hurrell et al., 2013) was run here as a single-column model (SCM). SCMs are used to evaluate climate model parameterizations (Randall et al., 1996; I. N. Williams et al., 2016; Xie et al., 2004). An SCM represents a specific grid-cell of a full climate model, and would reproduce the same grid-cell climate if the time-varying advective tendencies and vertical velocities were prescribed to match those of the parent climate model. Under such forcing, modifications to the moist turbulence and land-surface parameterizations reveal the impacts of the parameterizations on climate prediction, excluding effects of interactions with resolved-scale circulations (Randall & Cripe, 1999).

Large-scale advective tendencies and vertical velocities (hereafter referred to as large-scale forcing) were prescribed from an observationally constrained model data product (Xie et al., 2004), such that the time series simulated in our SCM corresponds to the observed time series of large-scale weather patterns. The

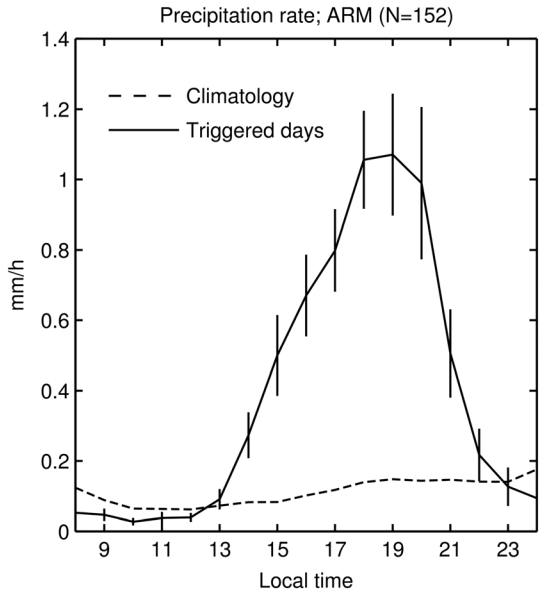

Figure 1. Diurnal cycle of observed precipitation on convective triggering days compared to climatology, for summer days (1 May to 1 September). Error bar widths are twice the standard error of the mean.
ARM = Atmospheric Radiation Measurement.

prescribed forcing is centered over the Atmospheric Radiation Measurement (ARM) site in the U.S. Southern Great Plains (SGP) and averaged over a 3° × 3° domain, which sets the effective size of the SCM grid cell. The size of the SCM grid reflects the resolution of the forcing data. Based on previous sensitivity tests using the same and higher-resolution forcing data (W. Lin et al., 2015), the SCM is not expected to be sensitive to the grid size.

The NCAR Community Atmosphere Model version 5.3 (CAM5; Neale et al., 2010) was used, which parameterizes deep convection according to the Zhang-McFarlane scheme (hereafter ZM; G. J. Zhang & McFarlane, 1995). Shallow convection and moist turbulence are represented by the University of Washington parameterizations (hereafter UW; Bretherton & Park, 2009; Park & Bretherton, 2009). In the ZM scheme, the mass-flux closure for cumulus convection is a function of convective available potential energy (CAPE), whereas in the UW parameterization it is a function of the ratio of convective inhibition energy (CIN) to cloud-base turbulent kinetic energy. A cloud macrophysics parameterization is used to diagnose stratiform cloud fractions and to integrate cloud processes across parameterizations (Park et al., 2014).

In all experiments, the Community Land Model (CLM4.0) was modified to have interannually varying monthly LAI inferred from 250-m Moderate Resolution Imaging Spectroradiometer (MODIS) retrievals (Riley et al., 2009) separated into plant functional types and aggregated to the model grid cell (I. N. Williams et al., 2016). The modified LAI is more realistic compared to the default climatological annual cycle of LAI prescribed in CLM4.0, and better represents the large fraction (35% of agricultural land) of winter crops in the SGP region. The land-model was spun-up offline until the soil moisture was equilibrated. The same timeseries of soil moisture was used to assign the land-model initial conditions in all experiments. Further details can be found in I. N. Williams et al. (2016).

For each experiment, the SCM was initialized with observational analyses at 12:00 UTC (7:00 local time) and run through the end of each summer day to produce a series of daily forecasts (1 May to 1 September) for years 1999–2014. Modeled tropospheric temperature and specific humidity were relaxed toward the observational analyses with a timescale of 6 hr. A four-member ensemble of simulations was formed using relaxation timescales of 3 and 6 hr, and by decreasing the lateral mixing efficiency parameter in the UW scheme from 8 to 4 to account for variations in lateral entrainment rates (Kuang & Bretherton, 2006; Park & Bretherton, 2009). The relaxation tendencies allowed temperature and specific humidity profiles to adjust to the surface forcing perturbations. The ensemble hindcasts were designed to generate larger samples from which to infer wet- and dry-advantage regime statistics. The resulting ensemble hindcasts were similar to each other in terms of the statistical distributions of triggering events across thermodynamic regimes (see section 4 for details).

Observational estimates of domain-mean atmospheric state variables were provided by the same data product used to prescribe the large-scale forcing in the SCM (Xie et al., 2004). Data from a network of 13 ARM surface heat flux stations (eddy covariance and energy balance Bowen ratio systems) were averaged over the 3° × 3° domain. The data were weighted to account for the fraction of the domain with the land-cover type represented by each station (Tang & Xie, 2015). The instruments are located in the flux footprints of the two dominant vegetation types (winter wheat and pasture or hay grasses) across the domain, which ensures that the important land cover types are well sampled.

Convective triggering events were defined as days with an afternoon (15:00–20:00 local time) precipitation maximum of at least 1 mm/hr (Y. Zhang & Klein, 2010), and required that the afternoon precipitation maximum be greater than at least twice that of the morning hours (Figure 1). The results were not sensitive to these thresholds, for example, similar results were obtained with a threshold of 0.5 mm/hr (F. Song & Zhang, 2017). Fair-weather days were defined as those having total daytime precipitation less than 0.01 mm. As in Y. Zhang and Klein (2010), a 4 km resolution gridded precipitation data set was used which

Table 1
Model Experiments Used in This Study (Indicating the Total Fraction of Triggering Days Relative to All Summer Days)

	Wet-soil perturbation	Dry-soil perturbation	Reference simulation
CLM-veg, ZM-on	0.16	0.14	0.15
CLM-veg, ZM-off	0.12	0.18	0.15
CLM-default, ZM-on	0.16	0.14	0.16
CLM-default, ZM-off	0.13	0.19	0.17

combines WSR-88D NEXRAD radar precipitation estimates and rain gauge reports (Breidenbach et al., 1998). In defining the triggering events, precipitation was averaged over a 50 km radius surrounding the ARM Central Facility site, to facilitate comparisons to vertically pointing cloud radar observations (described below). For the fair-weather days, the averaging was done over a 100 km radius to exclude days with precipitation in the SGP domain.

The Active Remotely-Sensed Cloud Locations (ARSCL) product was used, which identifies cloud layers every 10 s at 45 m vertical resolution, from zenith-pointing millimeter-wavelength and Ka-band ARM cloud radars (Clothiaux et al., 2000). Specifically, we used the ARM Best Estimate Cloud Radiation product, which estimates cloud fraction from the ARSCL based on the temporal frequency of radar-retrieved cloud layers within each hour (Xie et al., 2010).

PBL depth was estimated using the bulk-Richardson number method (McGrath-Spangler & Molod, 2014; Seidel et al., 2010). This allowed a consistent comparison between the modeled and observed PBL depth estimates using the same algorithm applied at the same spatial scale as the model (i.e., the SCM grid cell).

Model forcing and observational data were available for years 1999–2014. All analyses are based on these years.

3. Model Experiments

Twelve experiments were performed based on (1) perturbed soil moisture, (2) modified land-model parameterizations, and (3) modified convective parameterizations. Each combination that we explored is listed in Table 1.

The perturbed soil moisture experiments were run to assign observed days to wet- and dry-advantage regimes. The perturbations were based on the climatological maximum and minimum of soil moisture at each level in the soil column, respectively, using an offline reference simulation for the period 1980–2014 to derive the soil moisture statistics (Figure 2).

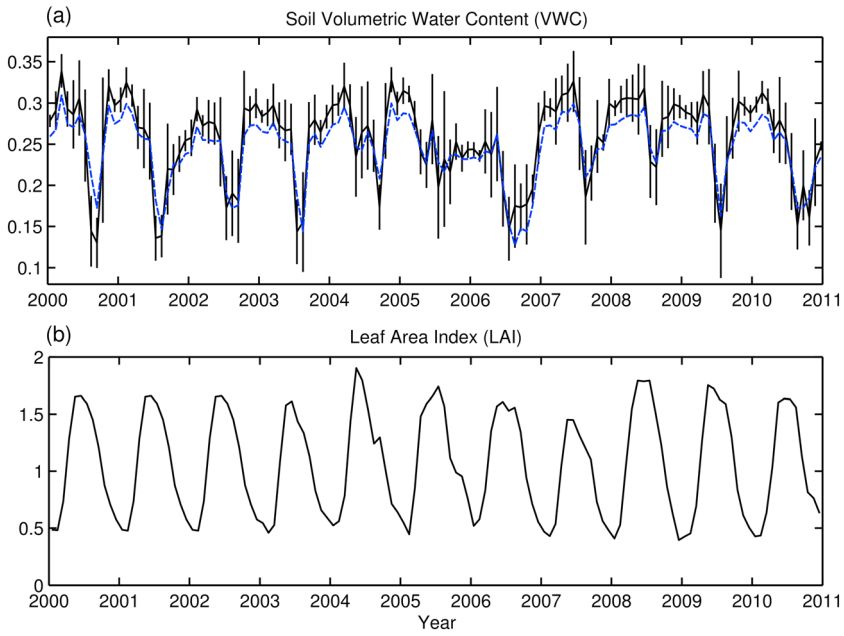

Figure 2. (a) Monthly soil volumetric water content for upper 10-cm (solid black) and 16–50 cm (dashed blue) layer averages for the reference experiments, and (b) prescribed total leaf area index for all experiments. Error bars in (a) indicate the standard deviation of the monthly mean.

The second set of experiments (CLM-veg) implemented the land-model parameter modifications in I. N. Williams et al. (2016) to explore the effects of weakening the coupling between soil moisture and ET (i.e., weakening the correlation between soil moisture and ET). Specifically, the modified parameters reduced the stomatal resistance to transpiration and increased the soil resistance to evaporation (by factors of 2–6 depending on the parameter), with the effect of increasing the fraction of transpiration in ET. As described in I. N. Williams et al. (2016) these changes led to greater overall ET during dry periods (including drought) and lower ET during wet periods relative to CLM-default but left the model climatological ET nearly unchanged.

The third set of experiments turned off the default ZM deep convection scheme in CAM5 (ZM-off). As shown later, the ZM-off configuration better predicts the diurnal cycle of cloud occurrence and "unmasks" the model sensitivity of deep convective clouds to land-surface state. Note that cumulus convection as represented by the UW shallow cumulus parameterization is not intrinsically limited to shallow clouds (Hohenegger & Bretherton, 2011), although the implementation in CAM5 has entrainment parameters that were chosen to best represent shallow cumulus. The ZM deep convective parameterization is called before the UW parameterization, such that turning the ZM parameterization off simply permits the UW scheme to develop its own deep cumulus. The UW scheme alone is not expected to realistically represent the precipitation processes in deep convection, which would require additional modifications to the parameterization (Park, 2014a, 2014b). Rather, the objective is to quantify the impact of the CAPE versus CIN-based mass flux closure.

The experiments were run with 30 vertical levels and a time step of 5 min, which improves the stability of the moist turbulence and cumulus parameterizations (Bretherton & Park, 2009).

4. Results

The fraction of all triggering days was calculated for each model experiment (Table 1). When aggregating all tropospheric states (regimes) together, only the experiments with ZM-off showed significant differences (at the 95% confidence level) between the wet- and dry-soil perturbation experiments. As shown later, the aggregated probabilities in Table 1 mask important regime-dependent responses to soil moisture perturbations. Additionally, the wet and dry soil moisture perturbations were large enough to overwhelm the effects of the stomatal and soil resistance parameter changes in CLM-veg, resulting in minor differences between CLM-veg and CLM-default. However, in what follows, the changes in CLM-veg are shown to be important in the intermediate states between soil moisture-limited and energy-limited ET.

The state-dependence of the results was analyzed by calculating an early-morning (7:00 local time) relative humidity index (hereafter RH*) and potential temperature gradient ($d\theta/dz$) averaged between 900 and 600 hPa in the lower-troposphere. RH* is the lower-tropospheric relative humidity evaluated at 1 km above the surface by fitting RH to a linear function of height between 600 and 900 hPa. These (or other, similar) indices are indicative of air that is entrained into the growing daytime PBL (Gentine et al., 2013). As expected, higher values of RH* and $d\theta/dz$ correspond to a more humid and stably stratified lower troposphere (Figure 3).

The state-dependence of the results was characterized by mapping the triggering events onto the $d\theta/dz$-RH* plane, to identify wet- and dry-advantage regimes (Figure 4). For example, the wet-advantage regime was defined based on the set of days in which triggering occurred in the wet-soil but not in the dry-soil perturbation experiment (e.g., blue circles in Figure 4). The results show a clear regime-dependence of triggering only in the ZM-off experiment, indicated by the shift in marginal distributions of stability. In contrast, the relationship between soil moisture and triggering (if any) in the ZM-on experiment is relatively insensitive to tropospheric regimes. In this sense, the ZM-on experiment is effectively a null hypothesis for the triggering feedback.

To generalize the definitions of wet- and dry-advantage regimes in terms of thermodynamic state, joint probability density functions were fitted to the distributions of wet- and dry-advantage days within the $d\theta/dz$-RH* phase space (data used for the fits are shown in Figure 4b). For example, the wet-advantage regime was assigned to days in which triggering events were at least twice as likely in the wet-soil experiments as in

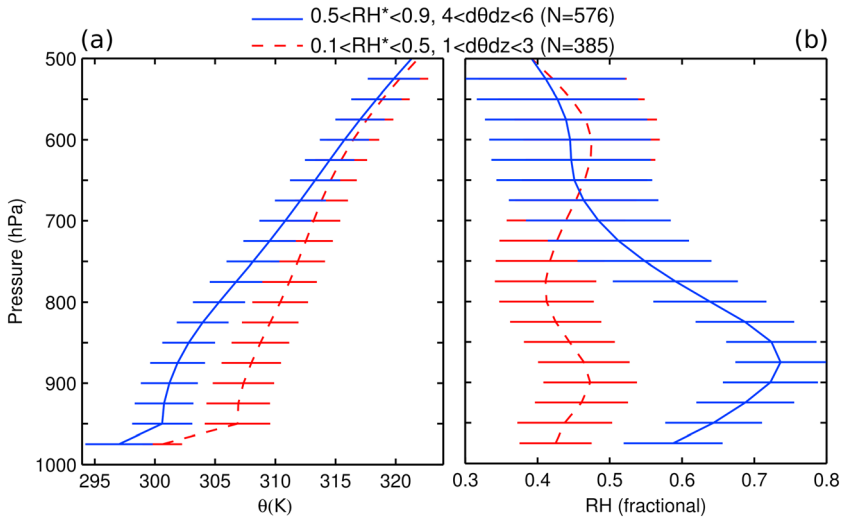

Figure 3. Average thermodynamic profiles for two contrasting sets of RH* and dθ/dz indices. (a) Potential temperature. (b) Relative humidity. Error bar widths indicate the standard deviation. RH* = relative humidity index.

the dry-soil experiments, based on the estimated probability density functions from the four ensemble members. Days when triggering was not at least twice as likely in one regime versus the other were considered to be atmospherically controlled. Lines dividing dry- and wet-advantage regimes (shown in Figure 5a) were derived from the interquartile range of lower-tropospheric stability (conditional on RH* bins) for those atmospherically controlled event-days.

Based on this approach, 23% of events were classified in wet-advantage regimes, while 27% were in dry-advantage regimes, and 50% of events were atmospherically controlled (i.e., they occurred in both the wet- and dry-soil perturbation experiments). There was no sensitivity of these percentages to relaxation timescale. Halving the lateral mixing efficiency parameter in the UW scheme reduced the percentage of dry-regime days from 27% to 23%. The results did not change by adding more ensemble members to the experiments (i.e., increasing from three to four ensemble members per experiment).

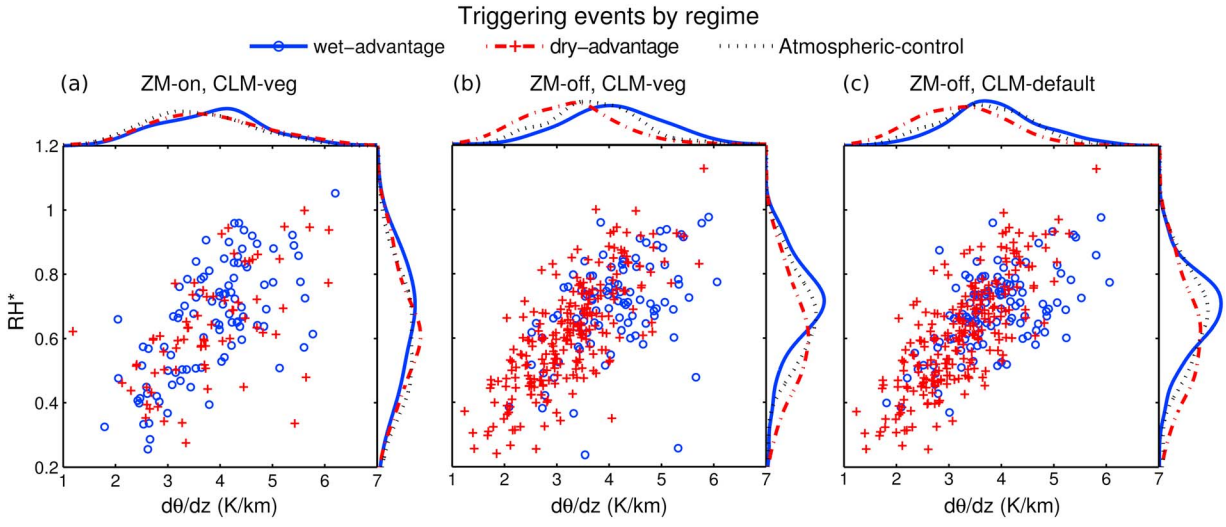

Figure 4. Triggering event distribution in the dθ/dz-RH* plane, for wet- and dry-advantage regimes (blue circles and red crosses, respectively) inferred from model experiments. (a) ZM-on/CLM-veg. (b) ZM-off/CLM-veg. (c) ZM-off/CLM-default. Each point represents an event-day. Marginal probability density functions are shown for wet- and dry-advantage regimes above each panel (blue and red lines, respectively). The marginal probability density functions of atmospherically controlled regimes are also shown (dotted black lines). Therefore, the ZM-off/CLM-veg experiments were used to define the wet- and dry-advantage regimes. Note that the results were not sensitive to the choice of land model parameters as shown by comparing CLM-veg to CLM-default (Figure 4c). RH* = relative humidity index.

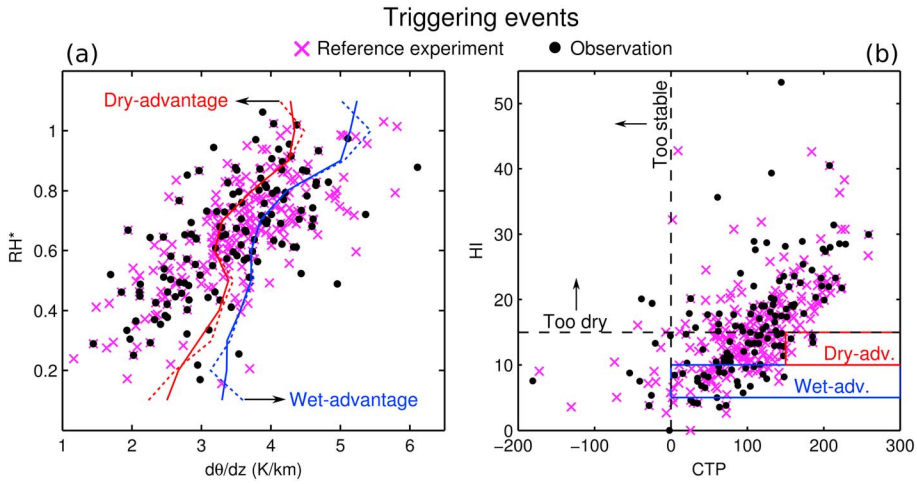

Figure 5. (a) Triggering event-days for reference experiments (ZM-off, CLM-veg; magenta crosshairs) and observations (black circles). Red and blue lines indicate the location of dry- and wet-advantage regimes derived from the perturbation soil moisture experiments, solid lines indicate regimes derived from CLM-veg, while dashed lines indicate CLM-default. (b) As in (a), but mapped onto the CTP-HI phase space of FE03. Boxes indicate the approximate locations of wet- and dry-advantage regimes and portions of the phase space thermodynamically unfavorable for precipitation in FE03. RH* = relative humidity index; HI = humidity index; CTP = convective triggering potential.

The present results were compared to the FE03 study by calculating the so-called convective triggering potential (CTP) and low-level humidity index (HI), which are similar to the dθ/dz-RH* coordinate above. Specifically, HI is a saturation deficit (dewpoint depression), while CTP is the difference between the temperature sounding and a moist adiabat; note that the directions of the CTP-HI axes are reversed relative to the dθ/dz-RH* axes; that is, stability increases with decreasing CTP, and humidity increases with decreasing HI. Interestingly, observed triggering events extend well beyond the thermodynamic limits deemed too stable or dry for precipitation in the FE03 study (Figure 5b), which indicates that the regime definitions can be highly model dependent. In particular, the humidity threshold of HI = 15 excludes many of the observed and modeled triggering events in our study, which suggests that it is too conservative. Qualitatively similar inferences were drawn from spatial and temporal statistics of soil moisture, precipitation, and CTP-HI (Ferguson & Wood, 2011; Roundy et al., 2012). Likewise, past studies have adjusted the thresholds for application to different regions and climates (Su et al., 2013; Tuinenburg et al., 2011).

Next, the above new regime definitions were used to form composite averages of events, to characterize observable signatures of the triggering feedback. As noted earlier, soil moisture was not perturbed in the reference experiments, to facilitate comparisons to observations. The daytime evolution of surface energy partitioning (i.e., EF) was compared between triggering days in wet- versus dry-advantage regimes, with the expectation that higher EFs would accompany triggering in wet-advantage regimes. It was further expected that the differences in EF between wet- and dry-advantage regimes (on triggering days) would be larger in the ZM-off experiments based on the above finding that ZM-on mutes the dependence of triggering on EF.

The experiments predict large differences in EF on triggering days, with lower EFs in dry-advantage regimes (Figure 6). However, the appearance of similar differences in EF in the ZM-on experiment (Figure 6a), with its lack of a significant triggering feedback, suggests that the occurrence of lower EFs in dry-advantage regimes is not entirely indicative of a causal link between EF and triggering outcomes. Comparing triggering days to fair-weather days did not help to control for such (noncausal) covariation, as indicated by the fact that both ZM-on and ZM-off experiments show lower EFs on triggering days than on fair-weather days (dashed lines in Figure 6a) in dry-advantage regimes. In addition, the predicted covariation between EF and regimes is overestimated compared to observations (Figure 6c) no matter which convective parameterization is used, which points to possible errors in the land model.

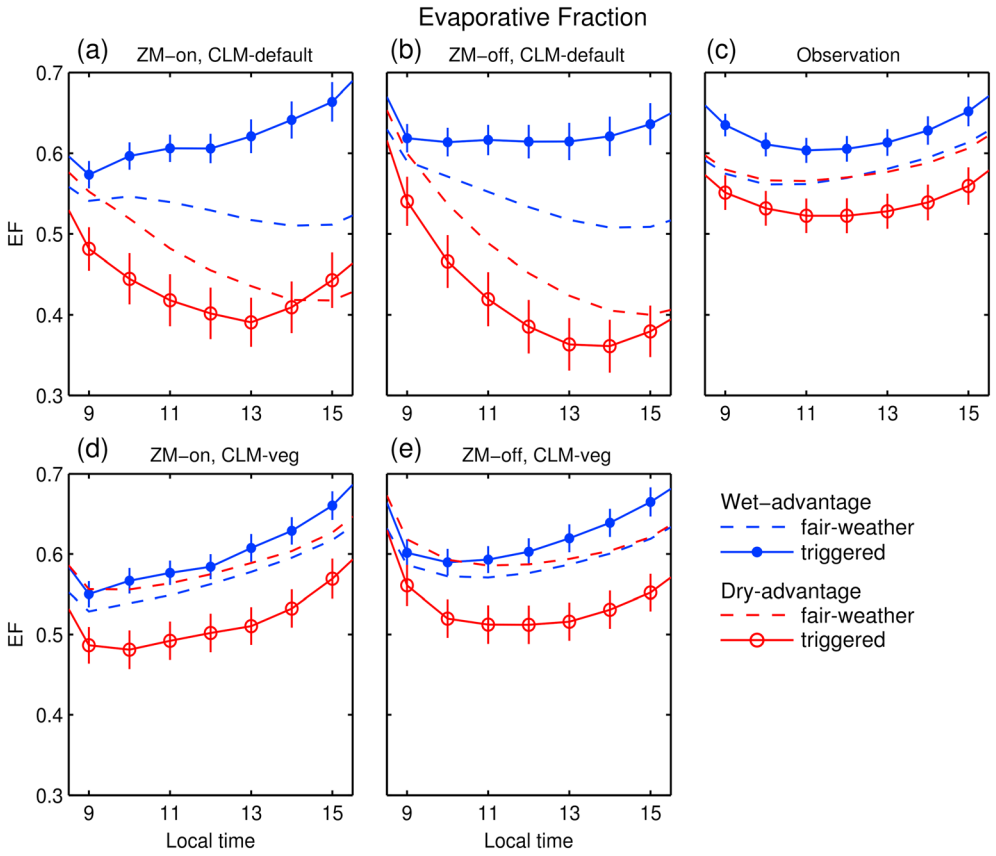

Figure 6. Partial diurnal cycles of EF on triggered (solid) and fair-weather (dashed) days, averaged over wet-advantage (blue) and dry-advantage (red) regimes. (a) ZM-on experiments. (b) ZM-off experiments. (c) Atmospheric Radiation Measurement observations. (d)–(e) as in (a)–(b) but using the modified CLM (CLM-veg). Error bar widths indicate twice the standard error of the mean. EF = evaporative fraction.

The two land model versions (CLM-veg and CLM-default) were compared to explore the role of land-model parameterizations, with the expectation that CLM-veg (with its reduced sensitivity of EF to soil moisture variations) would capture the muted regime-dependence of observed EF. Indeed, CLM-veg predicts smaller differences in EF between wet- and dry-advantage regimes, which better represents the observations (Figures 6d–6e). However, the daytime EFs remain similar between the ZM-off and ZM-on experiments, again indicating noncausal covariation between EF variations and triggering outcomes. Therefore, the relationship between EF and triggering outcomes by itself does not provide sufficient information to evaluate the hypothesized feedback mechanisms. The nature of the covariation between EF and triggering regimes is explored later in this section.

PBL depth and the difference between the PBL depth and the level of free convection (LFC; hereafter referred to as the PBL-LFC deficit) were analyzed to find a better (more causal) signature of the triggering feedback. Here we see much larger differences between the ZM-on and ZM-off experiments. Triggering in the dry-advantage regime involves PBL growth in both the ZM-off experiment and observations, but not in the ZM-on experiment (Figures 7a–7c). Likewise, the PBL-LFC deficit is smaller in the ZM-off experiments (and observations) in the hours leading up to the triggering events. These results indicate that, in a dry environment, air parcels are more likely to reach saturation via deeper lifting (and greater adiabatic cooling) by PBL eddies. Therefore, convective triggering is more likely with a lower surface EF, which produces a deeper PBL. Qualitatively similar results were obtained using CLM-default (not shown). Specifically, PBL depth was approximately 20 hPa deeper with CLM-default in the dry-advantage regime, which is consistent with the lower EF (higher sensible heating) in that model in the dry-advantage regime (compare Figures 6a and 6b).

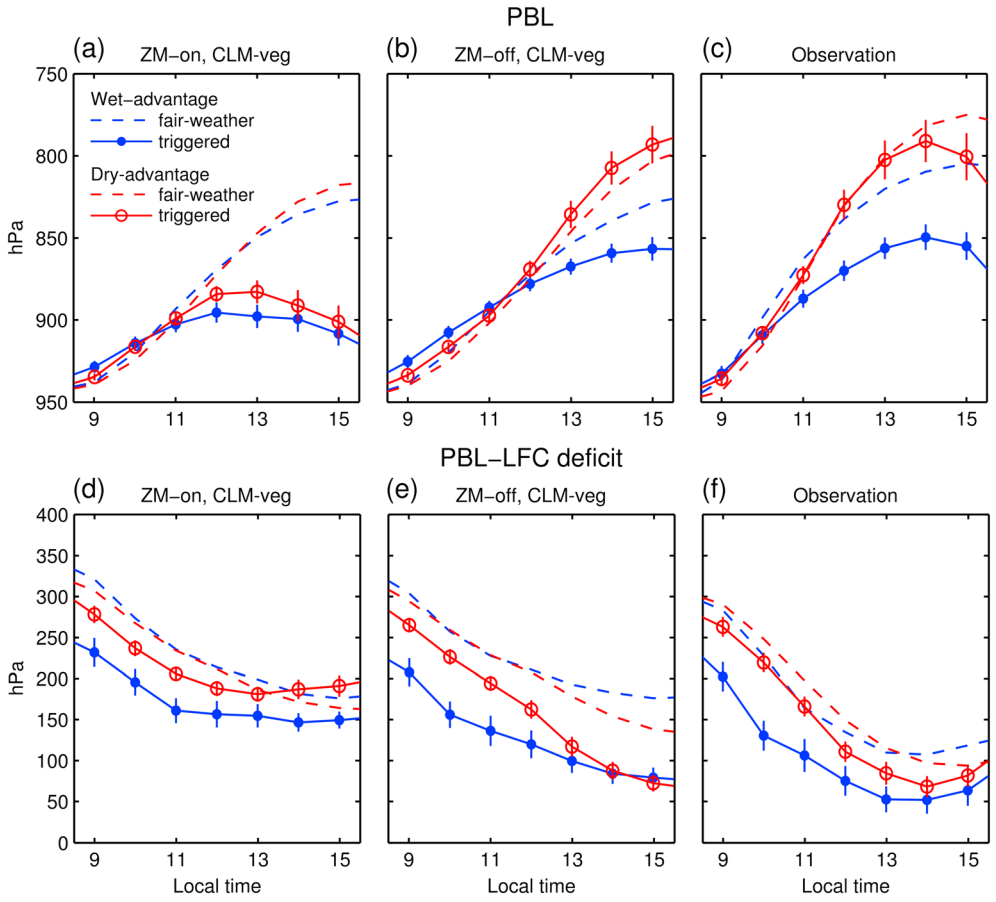

Figure 7. As in Figure 6, but for (a)–(c) PBL depth and (d)–(f) PBL-LFC deficit. PBL = boundary layer; LFC = level of free convection.

Next, the signature of triggering feedback mechanisms was explored in cloud observations, by partitioning ARSCL data into wet- and dry-advantage regimes, on triggered and fair-weather days. The probability of clouds was calculated at each pressure level (i.e., the frequency of occurrence of cloud fraction greater than 0). As expected, clouds extend deeper into the upper troposphere on triggering event days (Figures 8a–8b) and remain below the LFC on fair-weather days (Figures 8g–8h). The modest observed cloud probabilities (generally 0.2–0.5) are characteristic of scattered (short-duration) convection common in the early-afternoon in the SGP. The observations show fewer clouds and higher cloud bases in the dry-advantage regime (cf. Figures 8a and 8b). We also see delayed onset of boundary-layer clouds in the dry-advantage regime, on triggered and fair-weather days.

In contrast to the observations, ZM-on predicts deep clouds at nearly all hours of the day (Figures 8c–8d). The overestimation of deep cloud occurrence is worse in the dry-advantage regime and on fair-weather days (Figures 8i–8j), consistent with the well-known overactive trigger function in the ZM scheme. Biases in deep cloud frequency are partly alleviated by turning the ZM scheme off (Figures 8e–8f), which delays the initiation of deep clouds and reduces their frequency of occurrence (by nearly 50%). Similar improvements are seen on fair-weather days (Figures 8k–8l). Overall, the ZM-off experiments better capture the delayed onset and more rapid vertical development of deep clouds on dry-advantage days, as well as the suppression of deep clouds on fair-weather days.

The impact of land-model parameterization on cloud occurrence frequency was assessed by taking the difference in deep cloud frequency between the CLM-default and CLM-veg experiments with ZM-off. The results show up to 35% greater probability of deep clouds in the default CLM experiments for triggering days in the dry-advantage regime (Figure 9), indicating sensitivity of cloud probabilities to the land model. Triggering in the wet-advantage regime did not exhibit sensitivity to the land-model parameterizations

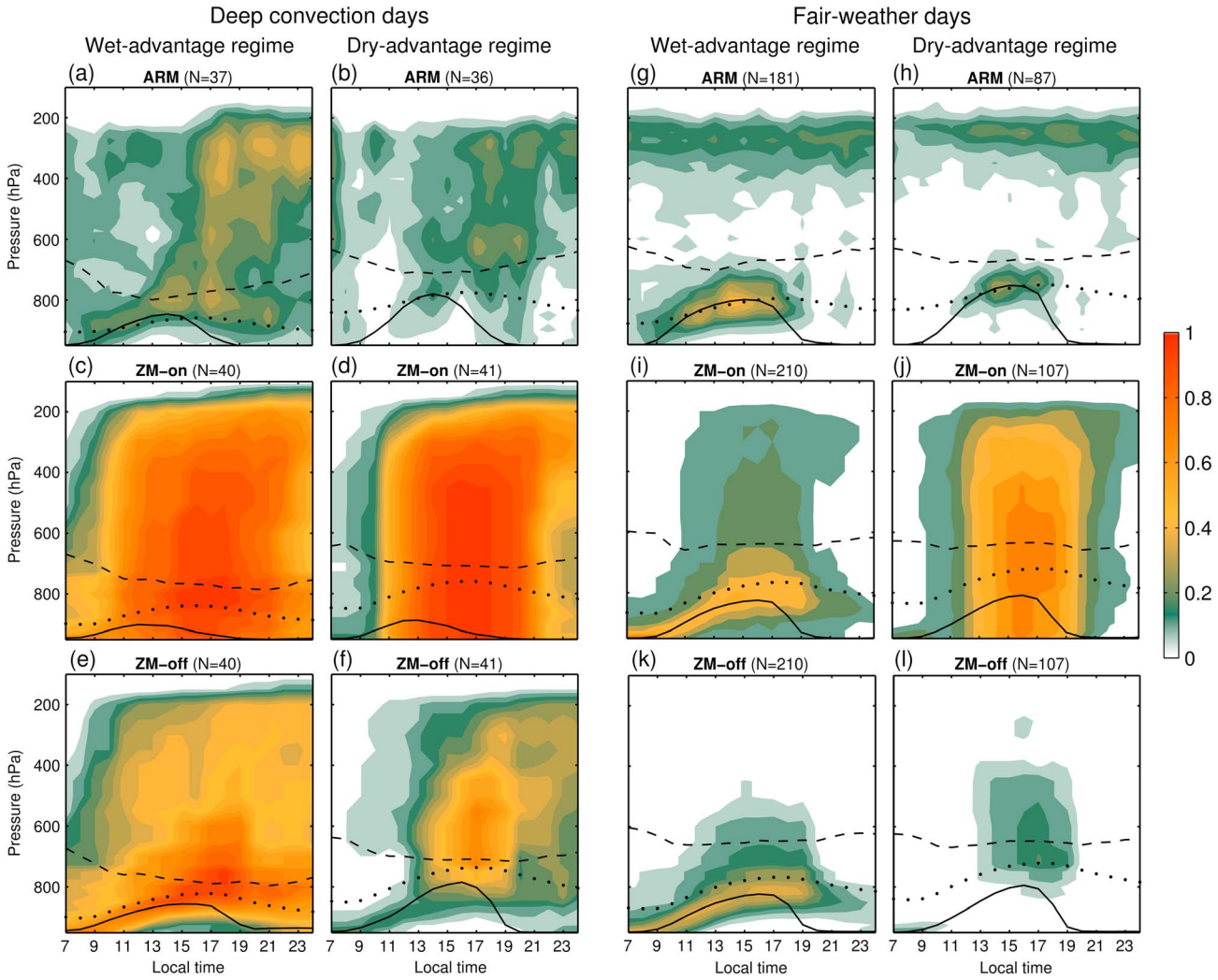

Figure 8. Cloud occurrence frequency diurnal cycles on triggered (left panels) and fair-weather (right panels) days. Also shown are boundary layer, lifted condensation level, and level of free convection pressure levels (solid, dotted, and dashed lines, respectively). (a)–(b) ARM observations of triggering events on wet- and dry-advantage days, respectively. (c)–(d) Reference experiments (CLM-veg, ZM-on). (e)–(f) Reference experiments (CLM-veg, ZM-off). (g)–(l) as in (a)–(f) but for fair-weather days. The number of samples (N) in each composite is indicated above each panel. ARM = Atmospheric Radiation Measurement.

(not shown), likely due to the much smaller differences in predicted EFs between CLM-default and CLM-veg in that regime. As noted above, a clear distinction in the timing and probability of deep clouds between wet- and dry-advantage regimes is evident only in the ZM-off experiments, which suggests that the ZM parameterization masks much of the sensitivity of convective triggering to variations in surface energy partitioning. This suggests that the ZM scheme could mask errors in the land-model.

This section returns to the questions raised earlier (from Figure 6) of why modeled EF is too low in the dry-advantage regime in CLM-default and, more generally, what determines the covariation between EF and triggering regimes. To address these questions, EF was projected onto the $d\theta/dz$-RH* phase space by linearly regressing EF onto the $d\theta/dz$-RH* plane using data for all summer days. An interaction term was included in the regression (i.e., $d\theta/dz \times$ RH*). The regression was performed for CLM-default, CLM-veg, and observations (contours in Figure 10). Comparing CLM-default (Figure 10a) to observations (Figure 10b) reveals that the underestimation of EF in CLM-default occurs in the lower RH* part of the phase space. Furthermore, the direction of the EF gradient in CLM-default is almost orthogonal to that in the observations, for the lower RH* half of the phase space. CLM-veg better represents the observed gradient.

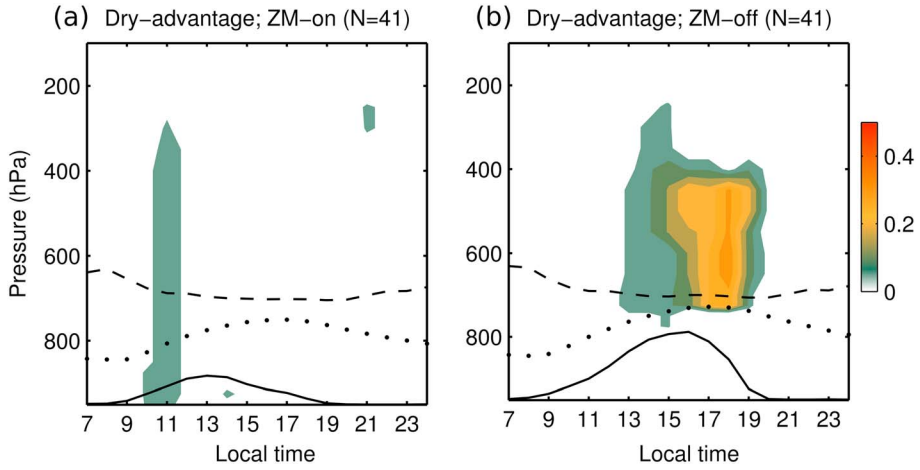

Figure 9. Difference in cloud occurrence frequency between land-model experiments (CLM-default minus CLM-veg), for triggering days in the dry-advantage regime. (a) ZM-on; (b) ZM-off. Also shown are the boundary layer (solid lines), lifted condensation level (dotted), and level of free convection (dashed) pressure levels of the reference simulation.

To further explore the causes of the different EF gradients in the dθ/dz-RH* plane, soil moisture and LAI were regressed onto the same dθ/dz-RH* plane (Figure 11). The similarity between the EF and soil moisture patterns (Figure 11a) suggests that EF in CLM-default is too sensitive to variations in soil moisture in the dry-advantage regime particularly for lower values of RH*. Not surprisingly, the gradient of EF in the CLM-veg configuration is less strongly aligned with that of soil moisture. The reduction in sensitivity of EF to near-surface soil moisture is an outcome of the increased resistance of bare-soil to evaporation and reduced stomatal resistance in CLM-veg, which increases the role of vegetation (LAI) in controlling EF (I. N. Williams et al., 2016). LAI does not strongly covary with RH* or dθ/dz (Figure 11b), which in part explains the muted variability of EF in the dθ/dz-RH* plane in CLM-veg.

Finally, the regime-dependent soil moisture-triggering feedback was evaluated in terms of the response of triggering event probability to EF (Figure 12). This is analogous to comparing the probabilities listed in Table 1 across wet- and dry-soil moisture perturbation experiments, but here the probabilities are conditional

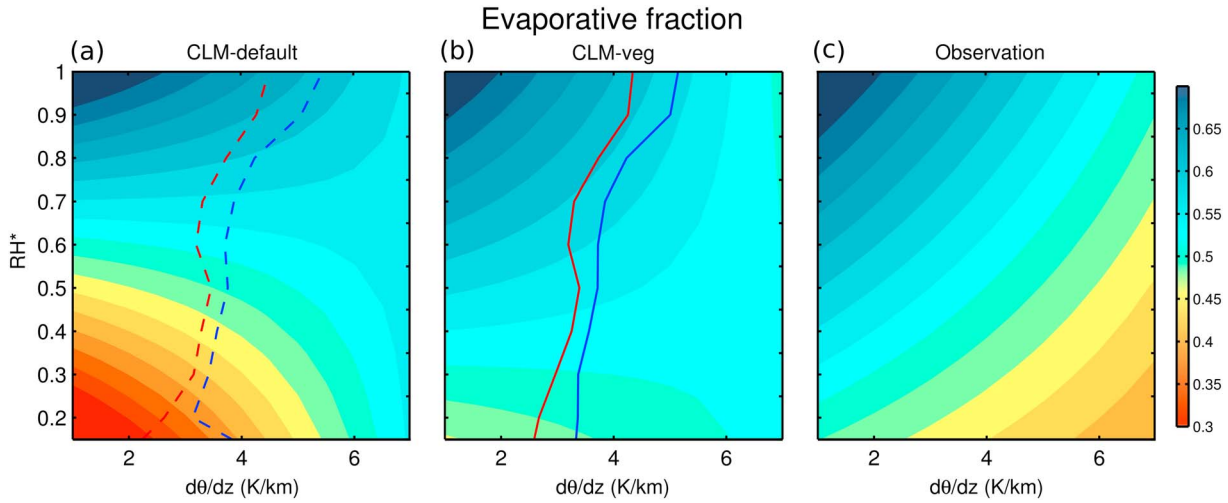

Figure 10. Daytime (10:00–14:00 local time) evaporative fraction linearly regressed onto the dθ/dz-RH* plane. (a) Default CLM. (b) CLM-veg. (c) Atmospheric Radiation Measurement observations. As in Figure 5a, red and blue lines indicate the location of dry- and wet-advantage regimes derived from the perturbation soil moisture experiments (solid lines indicate regimes derived from CLM-veg, while dashed lines indicate CLM-default). RH* = relative humidity index.

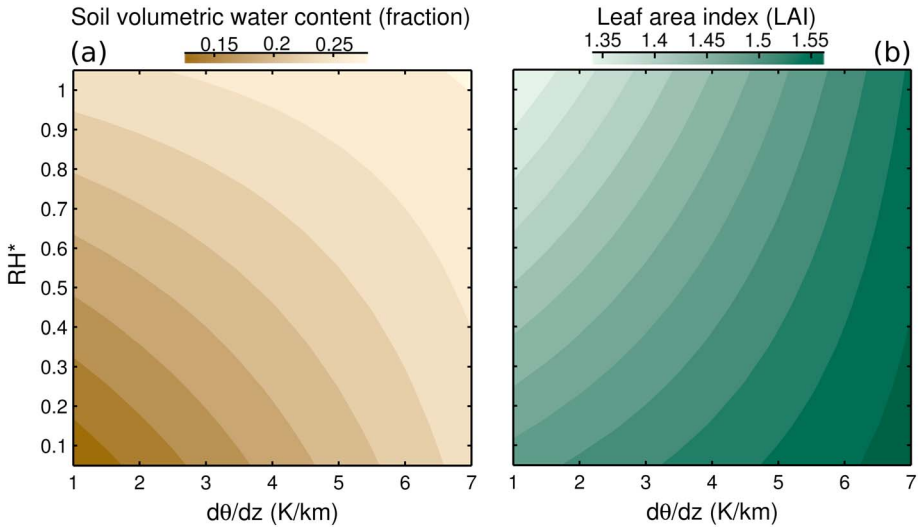

Figure 11. (a) Fractional soil volumetric water content initial condition and (b) LAI, linearly regressed onto the dθ/dz-RH* plane, for the reference experiments (both CLM-veg and CLM-default). Volumetric water content was averaged over the upper 10 cm of the soil column. RH* = relative humidity index; LAI = leaf area index.

on the wet- and dry-advantage regimes. In particular, the ZM-off model configurations show a systematic increase in triggering probability with decreasing EF in the dry-advantage regime, consistent with a negative feedback mechanism (Figure 12a). Likewise, there is a systematic increase in probability with increasing EF in the wet-advantage regime consistent with a positive feedback mechanism (Figure 12b). The probabilities were calculated as proportions (triggered events in each regime divided by the total number of triggered events in all regimes) to normalize for the overall higher probability of deep convection events in the model

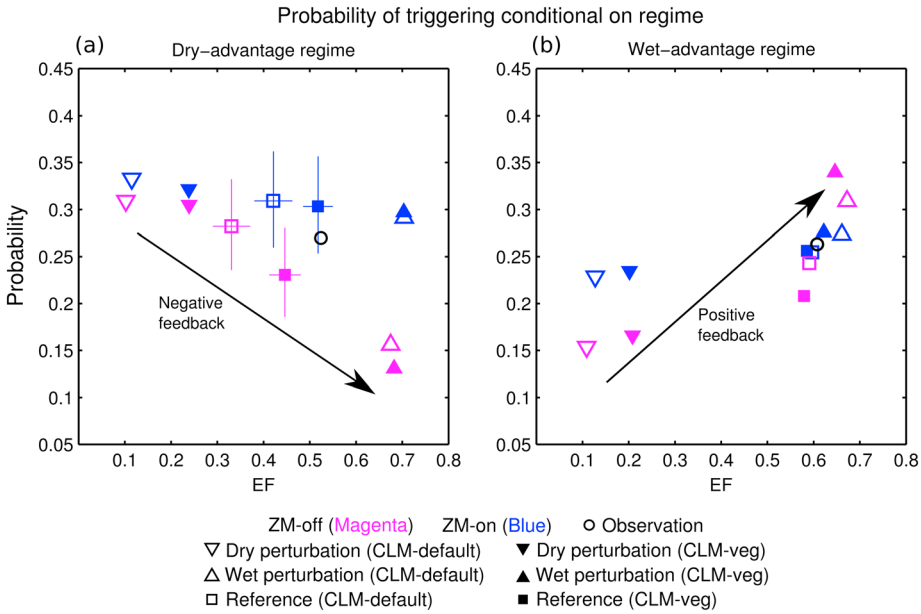

Figure 12. Probability of triggering events conditional on regime, shown as a function of average daytime (10:00–14:00 local time) EF for observations and the 12 model experiments corresponding to Table 1. (a) Dry-advantage regimes; (b) wet-advantage regimes. Probabilities are normalized by the total number of triggering events, to represent the proportion of triggering events in each regime. Error bars indicate the 95% confidence interval for EF and triggering event proportions (shown for reference experiments; other confidence intervals were similar). Arrows illustrate the direction of changes consistent with negative and positive soil moisture-triggering feedbacks. EF = evaporative fraction.

experiments relative to observations. These results highlight the importance of evaluating land-atmosphere feedbacks conditional on tropospheric state.

5. Discussion and Conclusions

In summary, convective triggering is not significantly influenced by soil moisture variations in the default version of CESM1.2, in the SGP. However, a systematic influence emerges after turning off the CAPE-based convective parameterization and allowing a CIN-based cumulus parameterization to represent deep convection. This suggests that the formulation of mass-flux closure affects modeled feedbacks between soil moisture and precipitation. Uncertainties in land-model parameterizations of ET also affect the probability of parameterized cumulus convection, and such impacts can be masked by errors in the deep convection scheme. Parameterizations which permit the triggering feedback mechanism better predict the statistics of daytime shallow and deep convection, in comparison to ARM observations. The results illustrate the benefits of testing and developing cumulus parameterizations in tandem with land-model parameterizations of surface fluxes.

The results show that the previously hypothesized regime-dependence of triggering feedbacks, seen in simple boundary-layer models (e.g., FE03 and others; Ek & Holtslag, 2004; Gentine et al., 2013), holds in more complex models having prescribed large-scale forcing, interactive radiation, and parameterized cloud dynamics. Consistent with FE03, the results here indicate two pathways of soil moisture influence on convective triggering. Lower EFs favor more vigorous dry turbulence and deeper PBLs, which can more effectively reach the lifted condensation level and LFC in dry environments where higher surface evaporation alone would be insufficient for surface or PBL-based parcels to reach saturation and become buoyant. On the other hand, the entrainment of warm air into the PBL lowers the relative humidity and thus counteracts the effects of adiabatic cooling at the PBL top. Likewise, it was found that triggering is favored by higher EFs and hence lower PBLs, in regimes with stronger dry stability (warmer air) just above the PBL.

The model experiments performed here predict that a larger portion (50%) of observed triggering events are influenced by variations in surface energy partitioning (and corresponding variations in land-surface state) than indicated in FE03. This difference is consistent with the broader distribution of triggering events in the experiments here, such that the wet- and dry-advantage regimes identified here span a wider range of tropospheric states compared to the regimes in FE03. A plausible explanation for this difference is that our SCM experiments represent the (parameterized) dynamics of cloudy plumes, which were not represented in FE03. Such dynamics include nonzero cloud-base vertical velocities that aid in triggering deep convection in regimes that are otherwise too dry or stable for deep convection (F. Song & Zhang, 2017). Another source of variation in the regimes is geographic location (Ferguson & Wood, 2011), which may influence tropospheric state in ways not fully captured by the stability and relative humidity metrics used here and in FE03.

This work tested feedbacks arising from responses of deep convection to temporal variations in soil moisture and EF. The positive and negative feedback mechanisms found in the SCM experiments here indicate that spatial variations in soil moisture are not necessary for such feedbacks, although they may be important in the real climate system (Taylor et al., 2012). The extent to which entraining plume parameterizations need to incorporate such heterogeneity effects can be explored by extending the experimental approach used here to convection-permitting models. In addition to soil moisture variations, the present findings show that vegetation processes (e.g., transpiration) are important in determining surface energy partitioning (C. A. Williams et al., 2012; I. N. Williams & Torn, 2015; Wilson et al., 2002). Specifically, errors in the representation of transpiration in land-surface models can propagate through the chain of coupled land-atmosphere processes to influence the statistics of convective clouds.

The state-dependence of the triggering feedback underscores the importance of evaluating convective and land-model parameterizations in contrasting states or regimes. The challenge of identifying so-called wet- and dry-soil moisture advantage regimes does not preclude such evaluations. This study provides an example of how model experiments can be combined with observations to shed light on complex soil moisture-precipitation feedbacks, by revealing their state-dependence. Integrative approaches such as these are needed to guide development of improved model parameterizations, to reduce uncertainties in projections of drought and precipitation extremes.

Acknowledgments
Three anonymous reviewers provided helpful comments and suggestions. Data were obtained from the Atmospheric Radiation Measurement (ARM) User Facility, a U.S. Department of Energy (DOE) Office of Science User Facility managed by the Office of Biological and Environmental Research. The atmospheric state and cloud profile data sets (sgparmbeatmC1 and sgparmbecldradC1) are available at https://doi.org/10.5439/1039931. The continuous forcing data (sgp60varanarucC1 and sgp60varanarapC1) are derived from the NOAA rapid update cycle (RUC; or rapid refresh, RAP) analysis data constrained with the ARM surface and TOA measurements (Xie et al., 2004). The data can be obtained at http://www.arm.gov/data/eval/29. The gridded precipitation data (sgpabrfcprecipX1) are available at http://www.archive.arm.gov/discovery/. This material is based upon work supported by the U.S. Department of Energy, Office of Science, Office of Biological and Environmental Research, Climate and Environmental Sciences Division, Atmospheric System Research Program, under Award Number DE-AC02-05CH11231.

References

Berg, A., Findell, K., Lintner, B. R., Gentine, P., & Kerr, C. (2013). Precipitation sensitivity to surface heat fluxes over North America in reanalysis and model data. *Journal of Hydrometeorology*, *14*(3), 722–743. https://doi.org/10.1175/jhm-d-12-0111.1

Betts, A. K. (2007). Coupling of water vapor convergence, clouds, precipitation, and land-surface processes. *Journal of Geophysical Research-Atmospheres*, *112*(D10). https://doi.org/10.1029/2006jd008191

Bonan, G. B., & Levis, S. (2006). Evaluating aspects of the community land and atmosphere models (CLM3 and CAM3) using a dynamic global vegetation model. *Journal of Climate*, *19*(11), 2290–2301. https://doi.org/10.1175/JCLI3741.1

Boussetta, S., Balsamo, G., Dutra, E., Beljaars, A., & Albergel, C. (2015). Assimilation of surface albedo and vegetation states from satellite observations and their impact on numerical weather prediction. *Remote Sensing of Environment*, *163*, 111–126. https://doi.org/10.1016/j.rse.2015.03.009

Breidenbach, J., Seo, D. J., Fulton, R. (1998). Stage II and III Post Processing of NEXRAD Precipitation Estimates in the Modernized Weather Service. AMS 78th Annual Meeting Phoenix, Arizona, January 1998.

Bretherton, C. S., & Park, S. (2009). A new moist turbulence parameterization in the community atmosphere model. *Journal of Climate*, *22*(12), 3422–3448. https://doi.org/10.1175/2008JCLI2556.1

Chen, L., Dirmeyer, P. A., Tawfik, A., & Lawrence, D. M. (2017). Sensitivities of land cover–precipitation feedback to convective triggering. *Journal of Hydrometeorology*, *18*(8), 2265–2283. https://doi.org/10.1175/JHM-D-17-0011.1

Cheruy, F., Dufresne, J. L., Hourdin, F., & Ducharne, A. (2014). Role of clouds and land-atmosphere coupling in midlatitude continental summer warm biases and climate change amplification in CMIP5 simulations. *Geophysical Research Letters*, *41*, 6493–6500. https://doi.org/10.1002/2014GL061145

Clothiaux, E. E., Ackerman, T. P., Mace, G. G., Moran, K. P., Marchand, R. T., Miller, M. A., & Martner, B. E. (2000). Objective determination of cloud heights and radar reflectivities using a combination of active remote sensors at the ARM CART sites. *Journal of Applied Meteorology*, *39*(5), 645–665. https://doi.org/10.1175/1520-0450(2000)039<0645:ODOCHA>2.0.CO;2

Couvreux, F., Rio, C., Guichard, F., Lothon, M., Canut, G., Bouniol, D., & Gounou, A. (2012). Initiation of daytime local convection in a semi-arid region analysed with high-resolution simulations and AMMA observations. *Quarterly Journal of the Royal Meteorological Society*, *138*(662), 56–71. https://doi.org/10.1002/qj.903

Dirmeyer, P. A. (2011). The terrestrial segment of soil moisture-climate coupling. *Geophysical Research Letters*, *38*, L16702. https://doi.org/10.1029/2011GL048268

Dirmeyer, P. A., Wang, Z., Mbuh, M. J., & Norton, H. E. (2014). Intensified land surface control on boundary layer growth in a changing climate. *Geophysical Research Letters*, *41*, 1290–1294. https://doi.org/10.1002/2013GL058826

Ek, M. B., & Holtslag, A. A. M. (2004). Influence of soil moisture on boundary layer cloud development. *Journal of Hydrometeorology*, *5*(1), 86–99. https://doi.org/10.1175/1525-7541(2004)005<0086:IOSMOB>2.0.CO;2

Eltahir, E. A. B. (1998). A soil moisture–rainfall feedback mechanism: 1. Theory and observations. *Water Resources Research*, *34*(4), 765–776. https://doi.org/10.1029/97WR03499

Ferguson, C. R., & Wood, E. F. (2011). Observed land–atmosphere coupling from satellite remote sensing and reanalysis. *Journal of Hydrometeorology*, *12*(6), 1221–1254. https://doi.org/10.1175/2011JHM1380.1

Findell, K. L., & Eltahir, E. A. B. (2003). Atmospheric controls on soil moisture-boundary layer interactions. Part I: Framework development. *Journal of Hydrometeorology*, *4*(3), 552–569. https://doi.org/10.1175/1525-7541(2003)004<0552:acosml>2.0.co;2

Findell, K. L., Gentine, P., Lintner, B. R., & Kerr, C. (2011). Probability of afternoon precipitation in eastern United States and Mexico enhanced by high evaporation. *Nature Geoscience*, *4*(7), 434–439. https://doi.org/10.1038/ngeo1174

Gentine, P., Holtslag, A. A. M., D'Andrea, F., & Ek, M. (2013). Surface and atmospheric controls on the onset of moist convection over land. *Journal of Hydrometeorology*, *14*(5), 1443–1462. https://doi.org/10.1175/jhm-d-12-0137.1

Guillod, B. P., Orlowsky, B., Miralles, D. G., Teuling, A. J., & Seneviratne, S. I. (2015). Reconciling spatial and temporal soil moisture effects on afternoon rainfall. *Nature Communications*, *6*(1), 6443. https://doi.org/10.1038/ncomms7443

Guillod, B. P., Orlowsky, B., Miralles, D., Teuling, A. J., Blanken, P. D., Buchmann, N., et al. (2014). Land-surface controls on afternoon precipitation diagnosed from observational data: uncertainties and confounding factors. *Atmospheric Chemistry and Physics*, *14*(16), 8343–8367. https://doi.org/10.5194/acp-14-8343-2014

Hohenegger, C., & Bretherton, C. S. (2011). Simulating deep convection with a shallow convection scheme. *Atmospheric Chemistry and Physics*, *11*(20), 10,389–10,406. Retrieved from http://www.atmos-chem-phys.net/11/10389/2011/. https://doi.org/10.5194/acp-11-10389-2011

Hohenegger, C., Brockhaus, P., Bretherton, C. S., & Schaer, C. (2009). The soil moisture-precipitation feedback in simulations with explicit and parameterized convection. *Journal of Climate*, *22*(19), 5003–5020. https://doi.org/10.1175/2009jcli2604.1

Hurrell, J. W., Holland, M. M., Gent, P. R., Ghan, S., Kay, J. E., Kushner, P. J., et al. (2013). The community earth system model: A framework for collaborative research. *Bulletin of the American Meteorological Society*, *94*(9), 1339–1360. https://doi.org/10.1175/BAMS-D-12-00121.1

Klein, S. A., Jiang, X., Boyle, J., Malyshev, S., & Xie, S. (2006). Diagnosis of the summertime warm and dry bias over the U.S. Southern Great Plains in the GFDL climate model using a weather forecasting approach. *Geophysical Research Letters*, *33*, L18805. https://doi.org/10.1029/2006gl027567

Koster, R. D., Suarez, M. J., Higgins, R. W., & Van den Dool, H. M. (2003). Observational evidence that soil moisture variations affect precipitation. *Geophysical Research Letters*, *30*(5), 1241. https://doi.org/10.1029/2002GL016571/full

Koster, R. D., Sud, Y. C., Guo, Z., Dirmeyer, P. A., Bonan, G., Oleson, K. W., et al. (2006). GLACE: The global land-atmosphere coupling experiment. Part I: Overview. *Journal of Hydrometeorology*, *7*(4), 590–610. https://doi.org/10.1175/JHM510.1

Kuang, Z., & Bretherton, C. S. (2006). A mass-flux scheme view of a high-resolution simulation of a transition from shallow to deep cumulus convection. *Journal of the Atmospheric Sciences*, *63*(7), 1895–1909. https://doi.org/10.1175/JAS3723.1

Lin, W., Liu, Y., Vogelmann, A. M., Fridlind, A., Endo, S., Song, H., et al. (2015). RACORO continental boundary layer cloud investigations: 3. Separation of parameterization biases single-column model CAM5 simulations of shallow cumulus. *Journal of Geophysical Research, D: Atmospheres*, *120*(12), 6015–6033. https://doi.org/10.1002/2014JD022524/full

Lin, Y., Dong, W., Zhang, M., Xie, Y., Xue, W., Huang, J., & Luo, Y. (2017). Causes of model dry and warm bias over central U.S. and impact on climate projections. *Nature Communications*, *8*(1), 881. https://doi.org/10.1038/s41467-017-01040-2

McGrath-Spangler, E. L., & Molod, A. (2014). Comparison of GEOS-5 AGCM planetary boundary layer depths computed with various definitions. *Atmospheric Chemistry and Physics*, *14*(13), 6717–6727. Retrieved from https://www.atmos-chem-phys.net/14/6717/2014/acp-14-6717-2014.pdf. https://doi.org/10.5194/acp-14-6717-2014

Neale, R. B., Chen, C.-C., Gettelman, A., Lauritzen, P. H., Park, S., Williamson, D. L., et al. (2010). Description of the NCAR community atmosphere model (CAM 5.0). NCAR Tech. Note NCAR/TN-486+ STR. Retrieved from https://www.ccsm.ucar.edu/models/ccsm4.0/cam/docs/description/cam4_desc.pdf

Park, S. (2014a). A unified convection scheme (UNICON). Part I: Formulation. *Journal of the Atmospheric Sciences*, *71*(11), 3902–3930. https://doi.org/10.1175/JAS-D-13-0233.1

Park, S. (2014b). A unified convection scheme (UNICON). Part II: Simulation. *Journal of the Atmospheric Sciences*, *71*(11), 3931–3973. https://doi.org/10.1175/JAS-D-13-0234.1

Park, S., & Bretherton, C. S. (2009). The University of Washington shallow convection and moist turbulence schemes and their impact on climate simulations with the community atmosphere model. *Journal of Climate*, *22*(12), 3449–3469. https://doi.org/10.1175/2008JCLI2557.1

Park, S., Bretherton, C. S., & Rasch, P. J. (2014). Integrating cloud processes in the community atmosphere model, version 5. *Journal of Climate*, *27*(18), 6821–6856. https://doi.org/10.1175/JCLI-D-14-00087.1

Qian, Y., Yan, H., Hou, Z., Johannesson, G., Klein, S., Lucas, D., et al. (2015). Parametric sensitivity analysis of precipitation at global and local scales in the community atmosphere model CAM5. *Journal of Advances in Modeling Earth Systems*, *7*, 382–411. https://doi.org/10.1002/2014MS000354

Qiao, F., & Liang, X.-Z. (2017). Effects of cumulus parameterization closures on simulations of summer precipitation over the continental United States. *Climate Dynamics*, *49*(1-2), 225–247. https://doi.org/10.1007/s00382-016-3338-6

Randall, D. A., & Cripe, D. G. (1999). Alternative methods for specification of observed forcing in single-column models and cloud system models. *Journal of Geophysical Research*, *104*(D20), 24,527–24,545. https://doi.org/10.1029/1999JD900765

Randall, D. A., Xu, K.-M., Somerville, R. J. C., & Iacobellis, S. (1996). Single-column models and cloud ensemble models as links between observations and climate models. *Journal of Climate*, *9*(8), 1683–1697. https://doi.org/10.1175/1520-0442(1996)009<1683:SCMACE>2.0.CO;2

Riley, W. J., Biraud, S. C., Torn, M. S., Fischer, M. L., Billesbach, D. P., & Berry, J. A. (2009). Regional CO2 and latent heat surface fluxes in the Southern Great Plains: Measurements, modeling, and scaling. *Journal of Geophysical Research*, *114*(G4). https://doi.org/10.1029/2009JG001003

Roundy, J. K., Ferguson, C. R., & Wood, E. F. (2012). Temporal variability of land–atmosphere coupling and its implications for drought over the Southeast United States. *Journal of Hydrometeorology*, *14*(2), 622–635. https://doi.org/10.1175/JHM-D-12-090.1

Santanello, J. A., Dirmeyer, P. A., Ferguson, C. R., Findell, K. L., Tawfik, A. B., Berg, A., et al. (2017). Land-atmosphere interactions: The LoCo perspective. *Bulletin of the American Meteorological Society*. https://doi.org/10.1175/BAMS-D-17-0001.1, *99*, 1253–1272.

Santanello, J. A., Peters-Lidard, C. D., & Kumar, S. V. (2011). Diagnosing the sensitivity of local land-atmosphere coupling via the soil moisture-boundary layer interaction. *Journal of Hydrometeorology*, *12*(5), 766–786. https://doi.org/10.1175/jhm-d-10-05014.1

Schär, C., Lüthi, D., Beyerle, U., & Heise, E. (1999). The soil–precipitation feedback: A process study with a regional climate model. *Journal of Climate*, *12*(3), 722–741. https://doi.org/10.1175/1520-0442(1999)012<0722:TSPFAP>2.0.CO;2

Seidel, D. J., Ao, C. O., & Li, K. (2010). Estimating climatological planetary boundary layer heights from radiosonde observations: Comparison of methods and uncertainty analysis. *Journal of Geophysical Research*, *115*(D16), 123. https://doi.org/10.1029/2009JD013680

Song, F., & Zhang, G. J. (2017). Improving trigger functions for convective parameterization schemes using GOAmazon observations. *Journal of Climate*, *30*(21), 8711–8726. https://doi.org/10.1175/JCLI-D-17-0042.1

Song, H.-J., Ferguson, C. R., & Roundy, J. K. (2016). Land–atmosphere coupling at the Southern Great Plains atmospheric radiation measurement (ARM) field site and its role in anomalous afternoon peak precipitation. *Journal of Hydrometeorology*, *17*(2), 541–556. https://doi.org/10.1175/JHM-D-15-0045.1

Su, H., Dickinson, R. E., Findell, K. L., & Lintner, B. R. (2013). How are spring snow conditions in Central Canada related to early warm-season precipitation? *Journal of Hydrometeorology*, *14*(3), 787–807. https://doi.org/10.1175/JHM-D-12-029.1

Sun, J., & Pritchard, M. S. (2016). Effects of explicit convection on global land-atmosphere coupling in the superparameterized CAM. *Journal of Advances in Modeling Earth Systems*, *8*, 1248–1269. https://doi.org/10.1002/2016MS000689

Tang, Q., & Xie, S. (2015). Station-based surface data value-added product (No. DOE/SC--ARM/TR-151). DOE Office of Science Atmospheric Radiation Measurement (ARM) Program (United States). doi:https://doi.org/10.2172/1238067

Taylor, C. M., de Jeu, R. A. M., Guichard, F., Harris, P. P., & Dorigo, W. A. (2012). Afternoon rain more likely over drier soils. *Nature*, *489*(7416), 423–426. https://doi.org/10.1038/nature11377

Tuinenburg, O. A., Hutjes, R. W. A., Jacobs, C. M. J., & Kabat, P. (2011). Diagnosis of local land–atmosphere feedbacks in India. *Journal of Climate*, *24*(1), 251–266. https://doi.org/10.1175/2010JCLI3779.1

Van Weverberg, K., Morcrette, C. J., Ma, H.-Y., Klein, S. A., & Petch, J. C. (2015). Using regime analysis to identify the contribution of clouds to surface temperature errors in weather and climate models: Cloud-regime analysis and surface temperature errors. *Quarterly Journal of the Royal Meteorological Society*, *141*(693), 3190–3206. https://doi.org/10.1002/qj.2603

Wang, J. K., Ford, T. W., & Quiring, S. M. (2015). Distinguishing between unorganized and organized convection when examining land–atmosphere relationships. *Journal of Applied Meteorology and Climatology*, *54*(11), 2229–2243. https://doi.org/10.1175/JAMC-D-15-0086.1

Wilcox, E. M., & Donner, L. J. (2007). The frequency of extreme rain events in satellite rain-rate estimates and an atmospheric general circulation model. *Journal of Climate*, *20*(1), 53–69. https://doi.org/10.1175/JCLI3987.1

Williams, C. A., Reichstein, M., Buchmann, N., Baldocchi, D., Beer, C., Schwalm, C., Wohlfahrt, G., et al. (2012). Climate and vegetation controls on the surface water balance: Synthesis of evapotranspiration measured across a global network of flux towers. *Water Resources Research*, *48*, W06523. https://doi.org/10.1029/2011WR011586

Williams, I. N., Lu, Y., Kueppers, L. M., Riley, W. J., Biraud, S. C., Bagley, J. E., & Torn, M. S. (2016). Land-atmosphere coupling and climate prediction over the US Southern Great Plains. *Journal of Geophysical Research, D: Atmospheres*, *121*(20). Retrieved from https://doi.org/10.1002/2016JD025223/full

Williams, I. N., & Torn, M. S. (2015). Vegetation controls on surface heat flux partitioning, and land-atmosphere coupling. *Geophysical Research Letters*, *42*, 9416–9424. https://doi.org/10.1002/2015GL066305

Wilson, K. B., Baldocchi, D. D., Aubinet, M., Berbigier, P., Bernhofer, C., Dolman, H., et al. (2002). Energy partitioning between latent and sensible heat flux during the warm season at FLUXNET sites. *Water Resources Research*, *38*(12), 1294. https://doi.org/10.1029/2001WR000989

Xie, S., Cederwall, R. T., & Zhang, M. (2004). Developing long-term single-column model/cloud system–resolving model forcing data using numerical weather prediction products constrained by surface and top of the atmosphere observations. *Journal of Geophysical Research*, *109*(D1). https://doi.org/10.1029/2003JD004045/full

Xie, S., McCoy, R. B., Klein, S. A., Cederwall, R. T., Wiscombe, W. J., Jensen, M. P., et al. (2010). Clouds and more: ARM climate modeling best estimate data: A new data product for climate studies. *Bulletin of the American Meteorological Society*, *91*(1), 13–20. https://doi.org/10.1175/2009BAMS2891.1

Yang, B., Qian, Y., Lin, G., & Leung, L. R. (2013). Uncertainty quantification and parameter tuning in the CAM5 Zhang-McFarlane convection scheme and impact of improved convection on the global circulation and climate. *Journal of Geophysical Research: Atmospheres*, *118*, 395–415. https://doi.org/10.1029/2012JD018213/full

Zhang, G. J., & McFarlane, N. A. (1995). Sensitivity of climate simulations to the parameterization of cumulus convection in the Canadian climate centre general circulation model. *Atmosphere: Ocean*, *33*(3), 407–446. https://doi.org/10.1080/07055900.1995.9649539

Zhang, Y., & Klein, S. A. (2010). Mechanisms affecting the transition from shallow to deep convection over land: Inferences from observations of the diurnal cycle collected at the ARM Southern Great Plains site. *Journal of the Atmospheric Sciences*, *67*(9), 2943–2959. https://doi.org/10.1175/2010JAS3366.1

Zhang, Y., & Klein, S. A. (2012). Factors controlling the vertical extent of fair-weather shallow cumulus clouds over land: Investigation of diurnal-cycle observations collected at the ARM Southern Great Plains site. *Journal of the Atmospheric Sciences*, *70*(4), 1297–1315. https://doi.org/10.1175/JAS-D-12-0131.1